TURBULENT SWIRLING FLOW IN ANNULAR DUCTS

M.A. Elkadi, Mofreh H. Hamed and F. Sh. Abou-Taleb

Mechanical Power Engineering Department, Faculty of Engineering
Menoufia University, EGYPT

ABSTRACT

A numerical study of fluid flow and heat transfer characteristics for fully developed turbulent air flow in a straight annular tube is presented. Two types of initial swirl profiles were used in the present numerical study. The effects of the swirl intensity and the annulus radius ratio on the flow and heat transfer parameters were studied. Computations were carried out for velocity distribution, turbulence parameters, friction losses and heat-transfer characteristics. The results show that with swirl generation the turbulence parameter, near the outer wall is higher than that in the inner wall and also the shear stress. The Nusselt number enhancement was higher for larger values of swirl intensities. Increasing the annulus radius ratio has shown increasing in Nusselt number enhancement. From the present results, empirical formulas have been deduced between the skin friction coefficient, Nusselt number and the Reynolds number with swirl intensity at the duct inlet. Comparison of present results with previous correlations has shown a fairly agreement.

Keywords: Turbulent flow, Annular duct, Swirl intensity and Nusselt number

INTRODUCTION

Turbulent swirling flow through longitudinal cylindrical annular ducts heated or unheated has many practical engineering applications such as in turbomachinery and heat exchangers. Many studies have been concerned with the flow in circular ducts with and without swirl. Little attention has been paid to turbulent curved flows with three dimensional influences. Study of turbulent swirling flow through an annulus primarily requires a knowledge of the velocity profiles and the effect of streamline curvature upon heat transfer and fluid flow characteristics. Swirling flow through annular pipes is a highly complex turbulent flow and is still challenging to predict. Several interesting effects appear in the flow field with introduction of swirl. For example, swirl is responsible for increasing shear rates, greater turbulence production and longer path lengths for a particular fluid particle so that the effect of swirl leads to an increase in heat transfer rates significantly over those found in purely axial pipe flow.

The pioneering works of Rothfus, *et al.* [1] and [2] have indicated that the need for the radius ratio as a correlating parameter and the use of outer zone parameter have been adopted in this type of flow. Kundensen and Katz [3] have shown that the hydraulic diameter is insufficient to correlate frictional pressure drop for laminar flow in annuli. An improvement in the calculation of turbulent friction in smooth concentric annuli have been shown by Jones and Leung [4]. They demonstrated that the theoretically determined laminar equivalent diameter which provides similarity in laminar flow for round tubes and concentric annuli, also, provides similarity in turbulent flow. Singh, *et al.* [5] have shown the flow characteristics in the two regions of the annulus. The stress in the inner region is higher than that in the outer region which may be explained by a higher value of velocity fluctuation in the inner

region and a smaller wall area. Also, the energy loss per unit volume is higher in the inner region due to higher turbulence. Okiishi and Serovy [6] conducted theoretical analysis of developing and fully developed turbulent flow of Newtonian fluid through a concentric annular passage supported by experimental data. They have shown the dependence of flow development on the geometry of the entrance. Furthermore, an appropriate turbulent velocity profile and relationships for friction factor in annulus and entrance region pressure drops are developed. Scott [7], has presented an analytical solution of the incompressible linearized swirl equation in annular flow. The results show for a constant value of effective viscosity $\mu_{eff.}$ and a slug axial velocity profile, the initial free vortex character is rapidly lost. The radial location of the maximum swirl velocity moves from the wall to r/r_o value of 0.67. Yeh and Philadephia [8], studied the development of incompressible turbulent boundary layer along stationary annular walls analytically and experimentally for a swirling flow. Study of fully developed temperature field and the mean velocity profile in turbulent liquid flow through a vertical concentric annular channel has been conducted by Roy, *et al.* [9]. Mattingly and Gordon [10], have made an extensive experimental investigation of the mixing behaviour of co-annular streams with substantial swirl present. Enhanced radial mixing is created as a result of the Rayleigh instability which itself is present because of the outwardly decreasing angular momentum of the fluid.

The present investigation is concerned with the theoretical study of swirl flow through concentric annulus. Swirling flow characteristics and heat transfer parameters are the main object of the present study. Variation of the inlet swirl velocity profile, swirl intensities and the annulus radius ratio are predicted.

FORMULATION OF GOVERNING EQUATIONS AND MATHEMATICAL MODELS

In this section, the formulation of the governing equations which include the continuity, momentum, stagnation enthalpy and turbulence equations together with their boundary conditions, including the effect of swirl on wall functions, are presented.

The Governing Equations

The set of turbulent Reynolds equations of conservation of mass, momentum and stagnation enthalpy in combination with turbulence kinetic energy (k) and turbulence dissipation rate (ε), which govern the two-dimensional axisymmetric incompressible swirling steady turbulent flow in a stationary annulus may be expressed in cylindrical coordinates as in References 11-13, (see Figure 1).

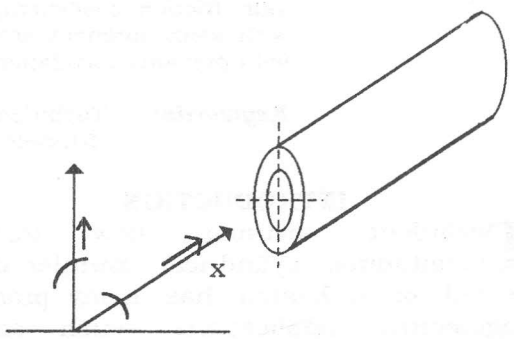

Figure 1 Geometry Coordinates

Continuity

$$\frac{\partial}{\partial x}(\rho u)+\frac{1}{r}\frac{\partial}{\partial r}(\rho\, vr)=0.0 \qquad (1)$$

Axial momentum

$$\frac{\partial}{\partial x}\left(\rho u^2\right)+\frac{1}{r}\frac{\partial}{\partial r}(\rho rvu)-\frac{\partial}{\partial x}\left(\mu_{eff}\frac{\partial u}{\partial x}\right)$$

$$-\frac{1}{r}\frac{\partial}{\partial r}\left(r\,\mu_{eff}\frac{\partial u}{\partial r}\right)=-\frac{\partial p}{\partial x}+\frac{\partial}{\partial x}\left(\mu_{eff}\frac{\partial u}{\partial x}\right)+$$

$$\frac{1}{r}\frac{\partial}{\partial r}\left(r\,\mu_{eff}\frac{\partial v}{\partial x}\right) \qquad (2)$$

Radial momentum

$$\frac{\partial}{\partial x}(\rho uv)+\frac{1}{r}\frac{\partial}{\partial r}(\rho rv^2)-\frac{\partial}{\partial x}\left(\mu_{eff}\frac{\partial v}{\partial x}\right)$$
$$-\frac{1}{r}\frac{\partial}{\partial r}\left(r\mu_{eff}\frac{\partial v}{\partial r}\right)=-\frac{\partial p}{\partial r}+\frac{\partial}{\partial x}\left(\mu_{eff}\frac{\partial u}{\partial r}\right)+$$
$$\frac{1}{r}\frac{\partial}{\partial r}\left(r\mu_{eff}\frac{\partial v}{\partial r}\right)+\frac{\rho w^2}{r}-2\,\mu_{eff}\cdot\frac{v}{r^2} \qquad (3)$$

Tangential momentum

$$\frac{\partial}{\partial x}(\rho uw)+\frac{1}{r}\frac{\partial}{\partial r}(\rho rvw)-\frac{\partial}{\partial x}\left(\mu_{eff}\frac{\partial w}{\partial x}\right)-$$
$$\frac{1}{r}\frac{\partial}{\partial r}\left(r\mu_{eff}\frac{\partial w}{\partial r}\right)=-\frac{\rho vw}{r}-\frac{w}{r^2}\frac{\partial}{\partial r}(r\mu_{eff}) \qquad (4)$$

Enthalpy

$$\frac{\partial}{\partial x}(\rho uh)+\frac{1}{r}\frac{\partial}{\partial r}(\rho rvh)-\frac{\partial}{\partial x}\left(\frac{\mu_{eff}}{\sigma_h}\frac{\partial h}{\partial x}\right)$$
$$-\frac{1}{r}\frac{\partial}{\partial r}\left(r\frac{\mu_{eff}}{\sigma_h}\frac{\partial h}{\partial r}\right)=0.0 \qquad (5)$$

Turbulence (K - ε) model

The turbulent diffusion fluxes which appear in the governing equations are modeled using Boussinesq approach in terms of the mean flow conditions and eddy diffusivities. These diffusivities are determined by solving additional conservation equations for the time-averaged kinetic energy of turbulence (k) and its dissipation rate (ε). The common form of the equations can be written as in References 13 and 14.

Turbulence kinetic energy Equation (k)

$$\frac{\partial}{\partial x}(\rho uk)+\frac{1}{r}\frac{\partial}{\partial r}(\rho rvk)-\frac{\partial}{\partial x}\left(\frac{\mu eff}{\sigma_k}\frac{\partial k}{\partial x}\right)$$
$$-\frac{1}{r}\frac{\partial}{\partial r}\left(r\frac{\mu eff}{\sigma_k}\frac{\partial k}{\partial r}\right)=G-C_D\rho\varepsilon \qquad (6)$$

Turbulence dissipation rate Equation (ε)

$$\frac{\partial}{\partial x}(\rho u\varepsilon)+\frac{1}{r}\frac{\partial}{\partial r}(\rho rv\varepsilon)-\frac{\partial}{\partial x}\left(\frac{\mu eff}{\sigma_\varepsilon}\frac{\partial \varepsilon}{\partial x}\right)-$$
$$\frac{1}{r}\frac{\partial}{\partial r}\left(r\frac{\mu eff}{\sigma_\varepsilon}\frac{\partial \varepsilon}{\partial r}\right)=\frac{\varepsilon}{k}(C_1G-C_2\rho\varepsilon) \qquad (7)$$

Where G is the production term given by:

$$G=\mu_{eff}\left\{\begin{array}{l}2\left(\left(\frac{\partial u}{\partial x}\right)^2+\left(\frac{\partial v}{\partial r}\right)^2+\left(\frac{v}{r}\right)^2\right)+\left(\frac{\partial w}{\partial x}\right)^2\\+\left(\frac{\partial u}{\partial r}+\frac{\partial v}{\partial x}\right)^2+\left(r\frac{\partial}{\partial r}\left(\frac{w}{r}\right)\right)^2\end{array}\right\} \qquad (8)$$

Within the above framework, the governing set of equations mentioned above may be compactly represented in terms of a single general equation for an arbitrary dependent variable φ :

$$\frac{1}{r}\left[\frac{\partial}{\partial x}(r\varphi u\rho)+\frac{\partial}{\partial r}(r\varphi v\rho)\right]=$$
$$\frac{1}{r}\left[\frac{\partial}{\partial x}\left(r\Gamma_\varphi\frac{\partial \varphi}{\partial x}\right)+\frac{\partial}{\partial r}\left(r\Gamma_\varphi\frac{\partial \varphi}{\partial r}\right)\right]+S_\varphi \qquad (9)$$

Where $\varphi \equiv 1$ for the continuity equation and for other equations , φ may stand for u,v,w,h,k, ε, etc. and Sφ is the corresponding source term which has various forms. Table 1 summarizes the values of these quantities.
Where, certain quantities are defined as follows:

$$S_u=\frac{\partial}{\partial x}\left[\mu_{eff}\frac{\partial u}{\partial x}\right]+\frac{1}{r}\frac{\partial}{\partial r}\left[r\mu_{eff}\frac{\partial v}{\partial x}\right]$$
$$S_v=\frac{\partial}{\partial x}\left[\mu_{eff}\frac{\partial u}{\partial r}\right]+\frac{1}{r}\frac{\partial}{\partial r}\left[r\mu_{eff}\frac{\partial v}{\partial r}\right]$$

Table 1 Conservation Equations Corresponding to Equation 9.

Conservation of	φ	Γ_φ	S_φ
Mass	1	0.0	0.0
Axial momentum	u	μ_{eff}	$-\frac{\partial p}{\partial x}+S_u$
Radial momentum	v	μ_{eff}	$-\frac{\partial p}{\partial r}+\frac{\rho w^2}{r}-\frac{2\mu_{etf}v}{r^2}+S_v$
Tangential momentum	w	μ_{eff}	$-\frac{\rho vw}{r}-\frac{w}{r^2}\frac{\partial}{\partial r}(r\mu_{eff})$
Kinetic energy	k	$\frac{\mu_{eff}}{\sigma_k}$	$G-C_D\rho\varepsilon$
Dissipation rate	ε	$\frac{\mu_{eff}}{\sigma_\varepsilon}$	$\frac{C_1G\varepsilon-C_2\rho\varepsilon^2}{k}$
Enthalpy	h	$\frac{\mu_{eff}}{\sigma_h}$	0.0

The effective viscosity μ_{eff} is given by:

$$\mu_{eff}=\mu+C_\mu\frac{\rho k^2}{\varepsilon} \qquad (10)$$

Where μ is the laminar viscosity.

The constants of the turbulence (k-ε) model C_μ, C_1, C_2, σ_h, σ_k and σ_ε are recommended as in References 13 and 16 which are given in Table 2.

Table 2 Turbulence model constants.

C_μ	C_1	C_2	σ_k	σ_ε	σ_h
0.09	1.43	1.92	1.0	1.3	0.9

Boundary conditions

Boundary conditions which must be specified on the entire boundary around the solution domain are, velocity components, temperature, (k) and (ε).

At the inlet

All variables are given definite fixed values (Dirichlet conditions), see Figure 2. The distribution of inlet velocity profile is assumed in the calculation as in Reference 15, as follows:

a- Uniform axial velocity profile with a flat swirl profile (plug flow). i.e $u = u_{in}$, $w = w_{in}$, ($w_{in} = u_{in} \tan\beta$) and $h = h_{in}$.

b- Uniform axial velocity with solid body rotation (forced vortex) i.e $u = u_{in}$, $w = \overline{w}_{in}\left(\frac{r-r_{in}}{r_{out}-r_{in}}\right)$ and $h = h_{in}$.

where, $\beta = \tan^{-1}(w/u)$

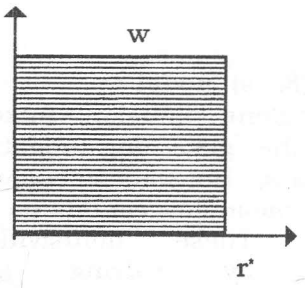

a- Inlet plug profile (Flat swirl)

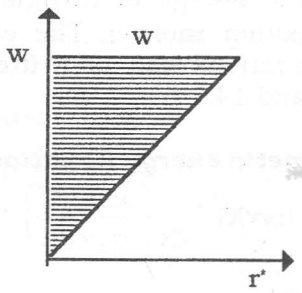

b- Inlet plug profile (Solid body rotation)

Figure 2 Inlet flow condition

At the outlet

At the outlet all variables are given zero normal gradient $\frac{\partial \varphi}{\partial x} = 0$ [Neumann conditions] except the radial velocity v which is set to zero

$$\left[\frac{\partial u}{\partial x} = \frac{\partial k}{\partial x} = \frac{\partial \varepsilon}{\partial x} = \frac{\partial h}{\partial x} = \ldots\ldots = 0\right]$$

At the wall

All velocity components u, v and w are given a value zero near the wall regions. Equations were introduced to link the values of dependent variables on the wall to those in the logarithmic region, taking into account the effect of swirl. The first grid point in the flow next to the wall is placed just outside the viscous Layer. At that point the resulting velocity V_p, parallel to the wall boundaries as shown in Figure 3 is given by [14]:

$$\frac{V_p}{u^+} = \frac{1}{\chi}\ell n\left[Ey_p^+\right] \qquad (11)$$

Where u^+ and y_p^+ are the friction velocity and the dimensionless wall distance defined respectively by:

$$u^+ = \sqrt{\frac{\tau_w}{\rho}} \quad , \quad y_p^+ = \frac{\rho y_p u^+}{\mu_t} \quad \text{and}$$

$$\mu_t = C_\mu \frac{\rho k^2}{\varepsilon}$$

Where τ_w is the wall shear stress, χ and E are the Von-Karmans constant and the roughness parameter given by Reference 14, for smooth walls, χ = 0.4 and E =9.0.

On a similar way of Reference 13, and with the assumption that the shear stress at the point p is approximately equal to the wall shear stress, leads to:

$$u^+ = C_\mu^{1/4}.\sqrt{k} \qquad (12)$$

$$\tau_w = \frac{\rho c_\mu^{1/4}\sqrt{k}}{\frac{1}{\chi}\ell n\left(Ey_p^+\right)} V_p \qquad (13)$$

$$\varepsilon_p = \frac{C_\mu^{0.75} k^{1.5}}{\chi\, y_p} \qquad (14)$$

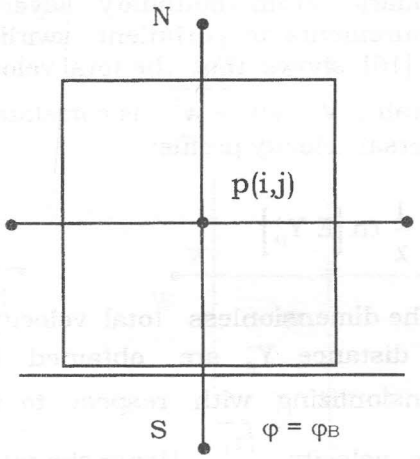

a- Wall φ - value on the bottom wall

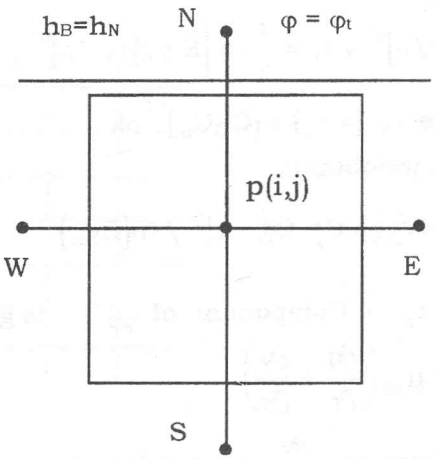

b- Wall φ - value on the top wall

Figure 3 Wall φ - distribution

Equations 12 to 14 give the values of k and ε at the nearst wall point P without solving the transport equations.

Wall functions and the effect of swirl

The effect of swirl on wall function specification is handled as follows:

The previous ideas are extended to find the total tangential shear stress near boundary. From boundary layer velocity measurements in turbulent, swirling, pipe flow [16] shows that the total velocity near the wall $V = \sqrt{u^2 + w^2}$ is correlated by the universal velocity profile:

$$V^+ = \frac{1}{\chi}\,\ell n\left[E\,Y_p^+\right]$$

The dimensionless total velocity V^+ and total distance Y_p^+ are obtained by non-dimensionlizing with respect to the total shear velocity $\sqrt{\frac{\tau_t}{\rho}}$. Hence the total shear stress at the wall $\tau_t = \sqrt{\tau_{rx}^2 + \tau_{r\theta}^2}$ is obtained from:

$$V\left[\tau_k / \rho\right]^{0.5} / \tau_t = \frac{1}{\chi}\,\ell n\left[E\,y_p\left[\tau_k / \rho\right]^{0.5} / \upsilon\right] \quad (15)$$

where $\tau_k\ (=\tau_t) = \left(C_D C_\mu\right)^{0.5}\rho k$

thus, we obtain:

$$\tau_t = -V_p \chi \rho\, C_\mu^{\frac{1}{4}}\, C_D^{\frac{1}{4}}\, k_p^{1/2} / \ell n\left(E y_p^+\right) \quad (16)$$

The τ_{rx} - Component of ?? is given by

$$\tau_{rx} = \mu_{eff}\left(\frac{\partial u}{\partial r} + \frac{\partial v}{\partial x}\right)$$

However, $\frac{\partial v}{\partial x}$ approaches zero and the boundary condition U_B = 0.0. Then the above wall function, Equation 15, is multiplied by the factor cos θ (= u/V) to obtain τ_{rx}, where θ is the angle between the total tangential velocity vector near the wall and the axial velocity vector. Then the wall function for u is:

$$\mu_{eff}\,\frac{\partial u}{\partial r} = \left[-\chi\,\rho\, C_\mu^{1/4}\, C_D^{1/4}\, k_p^{1/2} / \ell n\,(E Y_p^+)\right] u_p \quad (17)$$

Also the wall function for w is

$$\mu_{eff}\,\frac{\partial w}{\partial r} = \left\{-\chi\rho\, C_\mu^{1/4} C_D^{1/4} k_p^{1/2} / \left[\ell n\,(E\,Y_p^+)\right] + \frac{\mu_{eff}}{r}\right\} wp \quad (18)$$

Also the shear stress wall functions are employed for the (k) generation source (G) as follows:

$$G = 2\mu_{eff}\left[\left(\frac{\partial u}{\partial x}\right)^2 + \left(\frac{\partial v}{\partial r}\right)^2 + \left(\frac{v}{r}\right)^2\right] + \frac{\tau_t^2}{\mu_{eff}} + \mu_{eff}\left(\frac{\partial w}{\partial x}\right)^2 \quad (19)$$

where

$$\tau_t = \sqrt{\tau_{rx}^2 + \tau_{r\theta}^2} \quad \text{and,} \quad \tau_{rx} = \mu_{eff}\left(\frac{\partial u}{\partial r} + \frac{\partial v}{\partial x}\right)$$

$$\tau_{r\theta} = \mu_{eff}\left(\frac{\partial w}{\partial r} - \frac{w}{r}\right)$$

And also, in the present case the wall heat flux, q_s, with the boundary of $h_B = h_N$, was evaluated as in References 11 and 16:

$$\frac{-q_s}{\left(h_p - h_N\right)\rho\left|V_p\right|} = \frac{\tau_w / \left(\rho V_p^2\right)}{\sigma_{turb}\left[1 + p\sqrt{\left(\tau_w / \rho V_p^2\right)}\right]} \quad (20)$$

Where, $p = 9.0 \times \left[\frac{\sigma_{lam.}}{\sigma_{turb.}} - 1.0\right] \times \left(\frac{\sigma_{lam.}}{\sigma_{turb.}}\right)^{\frac{-1}{4}}$,

$\sigma_{lam.}$ and $\sigma_{turb.}$ are the laminar and turbulent Prandtl number.

THE FINITE- DIFFERENCE EQUATIONS AND SOLUTION PROCEDURE

The differential equations represented by Equation 9 and Table 1 were expressed in the finite difference form Reference 12. The finite difference equations for each φ are obtained by integrating Equation 9 over the appropriate control volume, Figure 4, centered about the location of φ and expressing the result in terms of neighboring and point values.

$$\sum_i \left(A_i - S_p'\right)\varphi_p = \sum_i A_i\varphi_i + S_p \qquad (21)$$

Where, $\sum_i$ summation over the four neighboring nodes N, E, W and S.

A_i's express effects of diffusion and convection.

The partial differential equations in the form of Equation 9 are expressed in the finite difference form and solved at the grid nodes resulting from grid lines scanning the flow filed. These finite difference equations are solved by the algorithm described by Patanker [12]. This algorithm is a series of steps of estimations and subsequent corrections of the pressure and velocities. To speed up the convergence and to prevent instability, under-relaxation factors are used. Figure 4 displays the calculation mesh and grid.

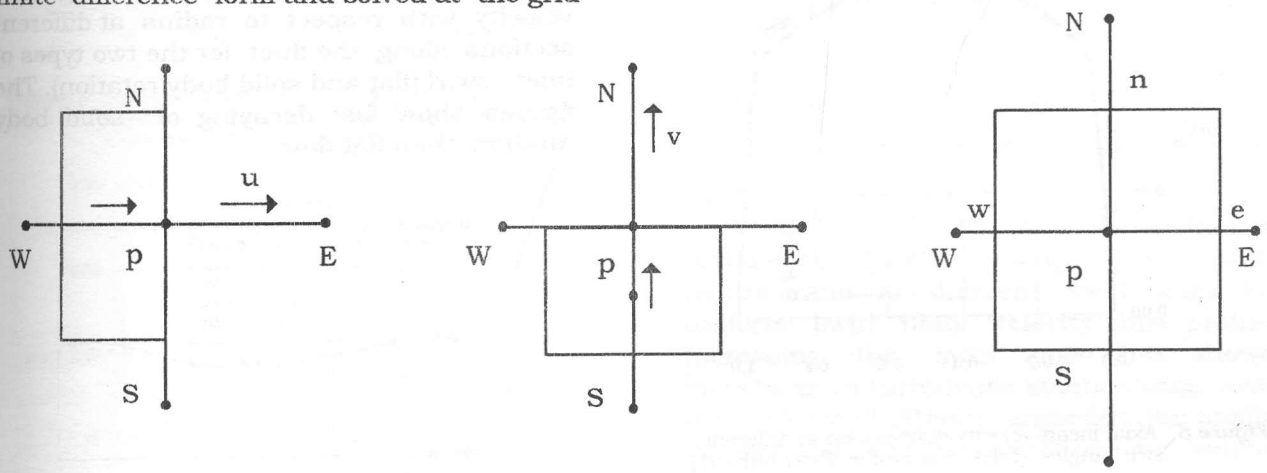

a-Control volume for cell for u b- Control volume for cell for v c- Control volume for cell for p,w,h,.....etc.

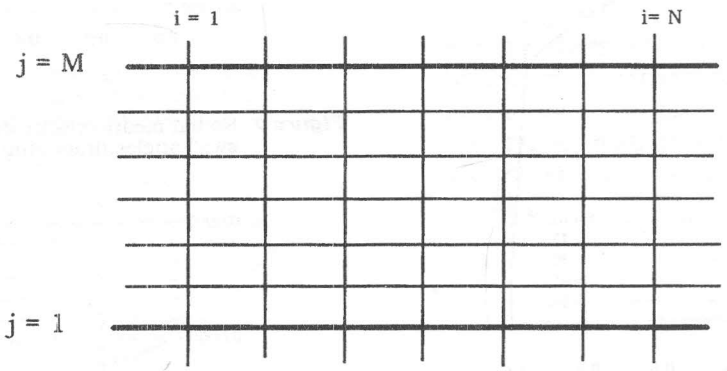

d- grid distribution

Figure 4 Control volumes and grid distribution

RESULTS AND DISCUSSION

The results have been simulated in two parts. The first is concerned with the results of flow characteristics with and without swirl. The second part is confined with the heat transfer parameters.

Mean Velocity Results

Mean axial velocity profiles have been shown in Figures 5 and 6. Introducing either plug (flat swirl) or solid body rotation flow into the main axial flow increased the mean axial velocity gradient near the outer

wall and the maximum velocity comes closer to the outer wall as the swirl angle increases. One observes a decrease in axial velocity at the inner wall of the duct for different swirl angles and at $\bar{x}$ = 41.26. This is referred to the effect of radial centrifugal force and thickening of boundary layer on the outer wall.

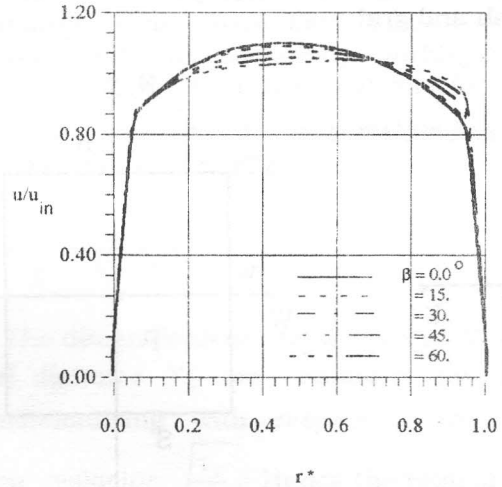

Figure 5 Axial mean-velocity distribution at different swirl angles. (inlet plug profile, Re=1.66E+05)

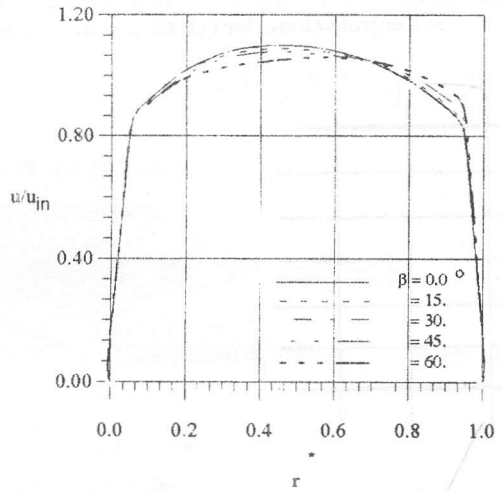

Figure 6 Axial mean-velocity distribution at different swirl angles. (inlet solid body rotation profile, Re=1.66E+05)

Figures 7 and 8 show the distribution of mean radial velocity at different swirl intensities. Increasing swirl intensity increased the negative value of the radial velocity. In addition, at no-swirl and 15° swirl angle the velocity profiles are showing a reduction near the outer wall. This behaviour of the radial velocity is referred to the unbalance between the centrifugal force and the radial pressure gradient created across the flow. Figures 9 and 10 show the distribution of swirl velocity component with respect to the radius ratio at different swirl intensities. Increasing the swirl angle increased the value of swirl velocity. Figures 11 and 12 show the decreasing of tangential velocity with respect to radius at different sections along the duct for the two types of inlet swirl (flat and solid body rotation). The figures show fast decaying of solid body rotation than flat flow.

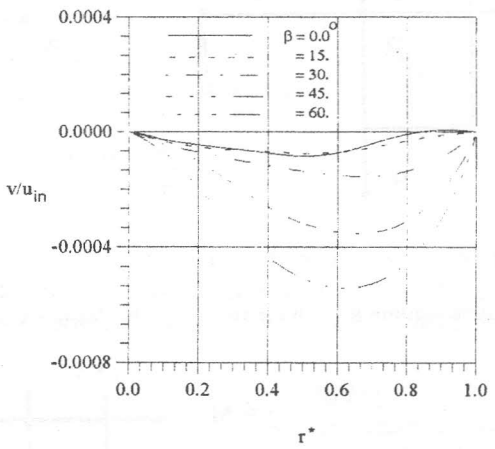

Figure 7 Radial mean-velocity distribution at different swirl angles.(inlet plug profile, Re=1.66E+05)

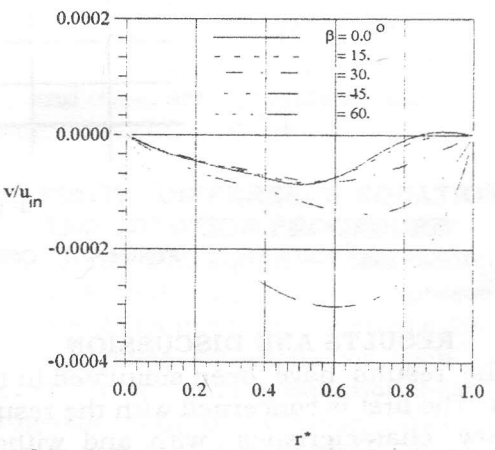

Figure 8 Radial mean-velocity distribution at different swirl angles. (inlet solid body rotation profile, Re=1.66E+05)

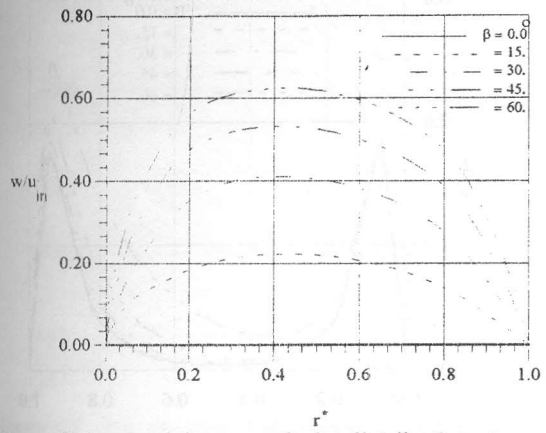

Figure 9 Tangential mean-velocity distribution at different swirl angles. (inlet plug profile, Re=1.66E+05)

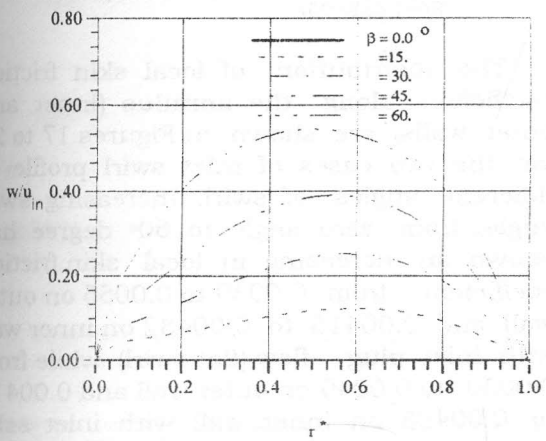

Figure 10 Tangential mean-velocity distribution at different swirl angles. (inlet solid body rotation profile, Re=1.66E+05)

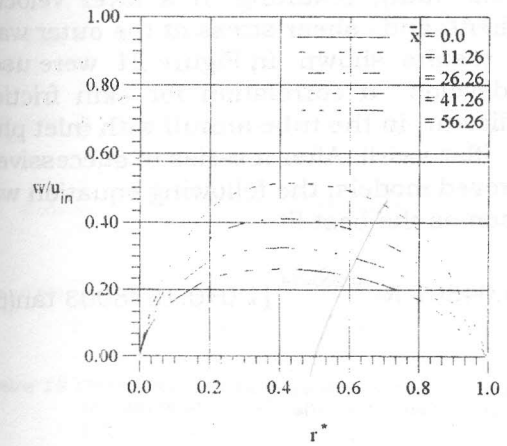

Figure 11 Tangential mean velocity distribution at different down stream locations. (inlet plug profile, Re=1.66E+05 & β=30.°)

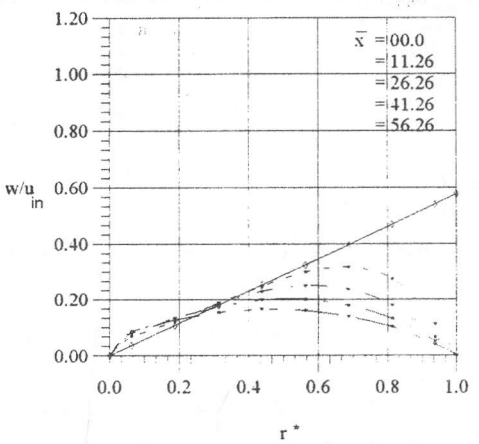

Figure 12 Tangential mean velocity distribution at different down stream locations.(inlet solid body rotation profile, Re=1.66E+05 & β=30.°)

Turbulence Results

Figure 13 shows the distribution of turbulence kinetic energy (T.K.E.) with radius ratio at different swirl angle for uniform swirl (flat) velocity inlet profile. Increasing the swirl angle has shown increasing in turbulence kinetic energy near the outer wall. At swirl angle 60° ,the profile is showing sharp increasing on kinetic energy from the inner wall to maximum value near the outer wall. Figure 14 shows the effect of introducing swirl, (solid body rotation) into the axial flow on total kinetic energy distribution. It shows a dip near the walls. Furthermore, increasing in turbulence kinetic energy is noticed near the outer wall at swirl angle 60 °, where the kinetic energy is doubled.

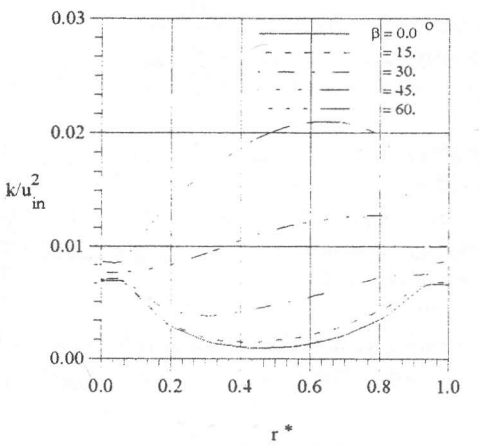

Figure 13 Distribution of T.K.E at different swirl angles. (inlet plug profile, Re=1.66E+05)

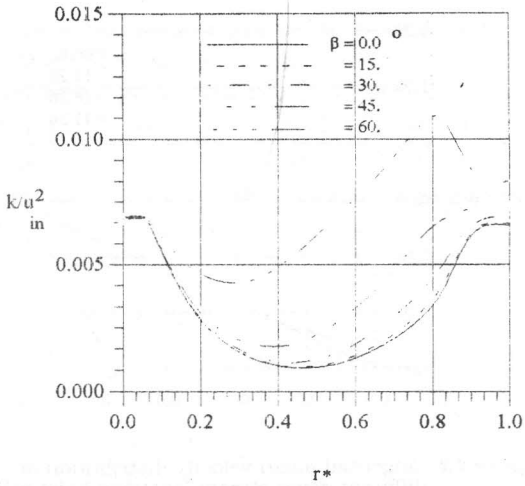

Figure 14 Distribution of T.K.E. at different swirl angles (inlet solid body rotation profile, Re=1.66E+05)

The distribution of turbulence energy dissipation (T.E.D.) with respect to radius ratio is profiled in Figures 15 and 16. The figures show higher energy dissipation near the walls. Furthermore, increasing in swirl angle is showing an increasing in energy dissipation near the outer wall. This is referred to increase of shear stress near the outer wall than at inner one. The results show that increasing in kinetic energy, turbulence intensities, energy dissipation and shear stress near the outer wall than inner wall. It is referred to the unbalance between centrifugal force and pressure gradient and unstability of flow.

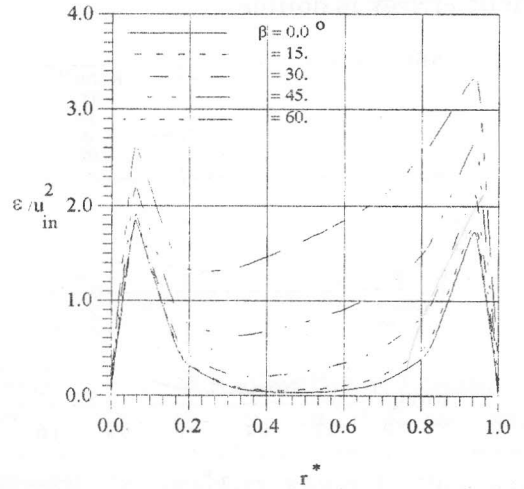

Figure 15 Distribution of T.E.D at different swirl angles.(inlet plug profile, Re=1.66E+05)

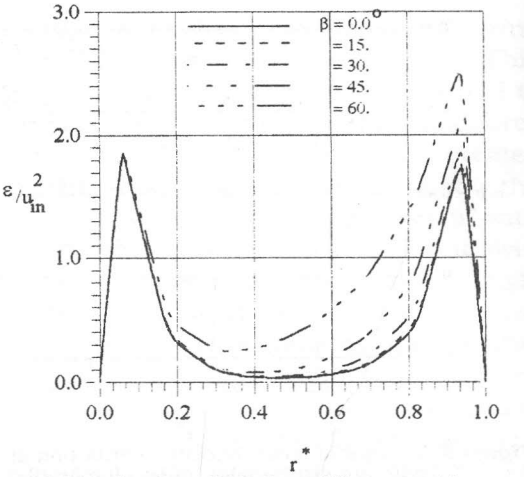

Figure 16 Distribution of T.E.D at different swirl angles.(inlet solid body rotation profile, Re=1.66E+05)

The distribution of local skin friction coefficient along the annulus (inner and outer walls) are shown in Figures 17 to 20 for the two cases of inlet swirl profile at different angles of swirl. Increasing swirl angle from zero angle to 60° degree has shown an increasing in local skin friction coefficient from 0.0039 to 0.0055 on outer wall and 0.00415 to 0.00482 on inner wall with inlet plug flow (flat swirl) while from 0.0039 to 0.0049 on outer wall and 0.00415 to 0.00423 on inner wall with inlet solid body rotation, at station $\bar{x} = 41.26$ along the duct. This is referred to that the mean velocity immediately adjacent to the wall is (pulled taut), resulting in a layer velocity gradient and shear stress at the outer wall. The results shown in Figure 21 were used to develop a correlation for skin friction coefficient in the tube annuli with inlet plug flow (flat swirl). After a series of successively improved models, the following equation was chosen as the best fit:

$$c_{f_t} = 0.04367\ R_e^{-0.200974}\ [1.0+0.1678003\ \tan(\beta)]$$

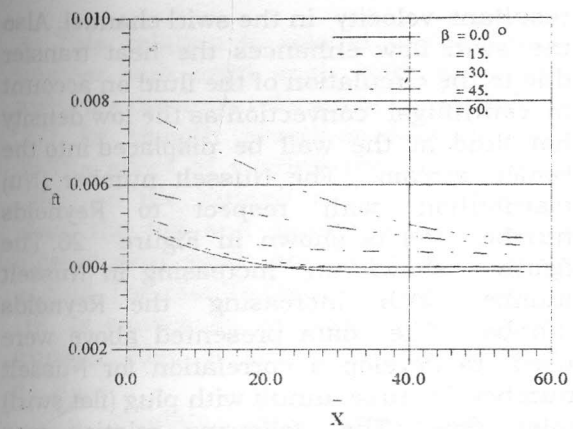

Figure 17 Distribution of skin friction coefficient along top wall at different swirl angles. (inlet plug profile, Re=1.66E+05)

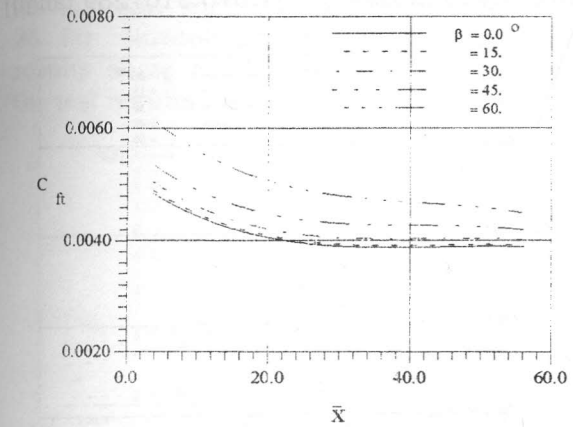

Figure 18 Distribution of skin friction coefficient along top wall at different swirl angles .(inlet solid body rotation profile, Re=1.66E+05)

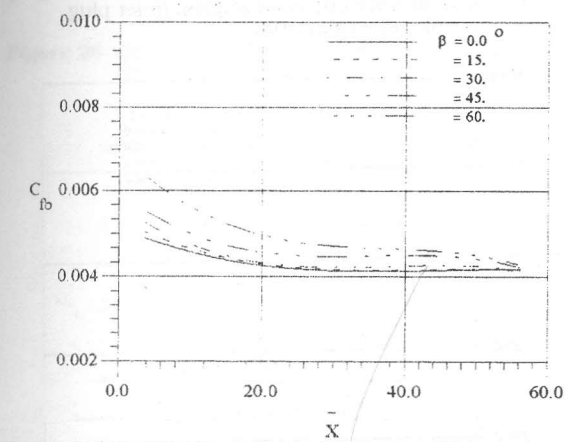

Figure 19 Distribution of skin friction coefficient along bottom wall at different swirl angles .(inlet plug profile, Re=1.66E+05)

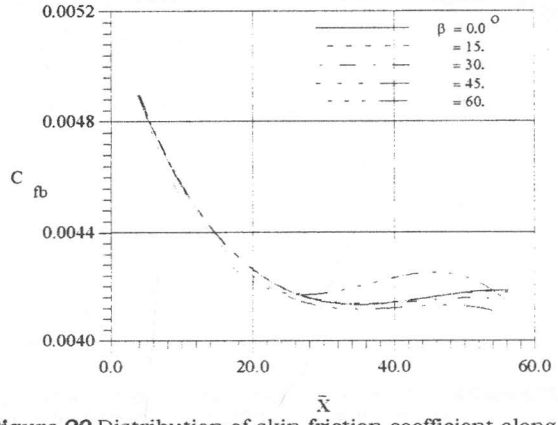

Figure 20 Distribution of skin friction coefficient along bottom wall at different swirl angles. (inlet solid body rotation profile, Re=1.66E+05)

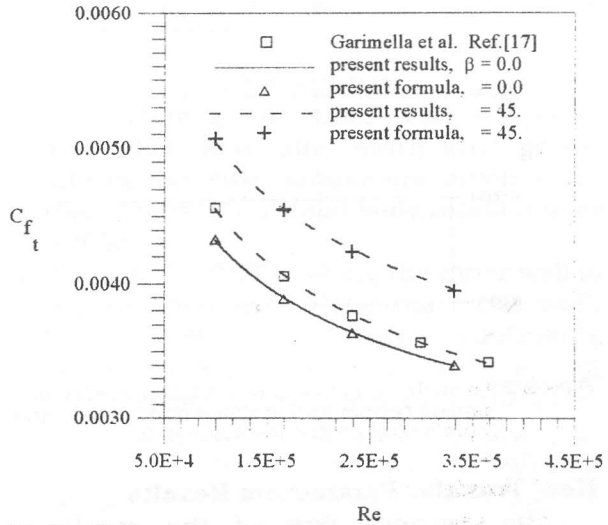

Figure 21 Comparison between skin friction coefficient and predicted by [17] (inlet plug profile).

This relation is related to the skin friction with swirl angle and is compared with the previous relation of Garimella *et al.* [17], for smooth annuli as shown in Figure 21.

The effect of varying the diameter ratio on the local skin friction coefficient distribution along the outer and inner wall of annular pipe at zero swirl are profiled in Figures 22 and 23. Increasing the aspect ratio has shown an increase in drag coefficient along the bottom wall. The same behaviour is shown on top wall but it appeared cross over at $\bar{x}$ = 41.26.

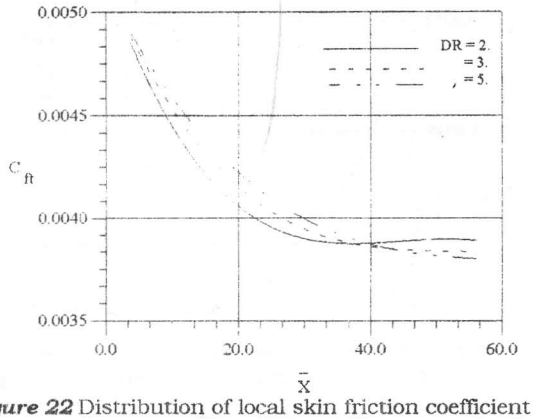

Figure 22 Distribution of local skin friction coefficient along top wall at different diameter ratio. (inlet plug profile, Re=1.66E+05)

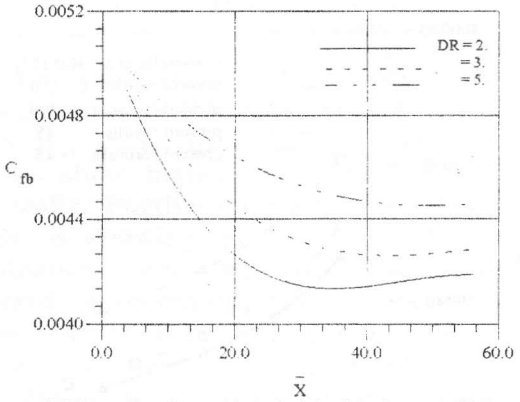

Figure 23 Distribution of local skin friction coefficient along bottom wall at different diameter ratio. (inlet plug profile, Re=1.66E+05)

Heat Transfer Parameters Results

The second part of the results is concerned with the calculation of heat transfer parameters for the flow of hot medium in smooth annular pipe.

Figures 24 and 25 show the distribution of Nusselt number (Nu) with respect to axial distance along the walls of annulus at different swirl intensities from zero swirl angle to 60° . Increasing swirl angle is showing an increase in Nusselt number (Nu) from 313 to 375 at station $\bar{x}$ = 1.5 with solid body rotation inlet profile while with plug (flat) swirl profile the Nusselt number is increased from 315 to 425. Increasing in swirl intensities are showing an increase in Nusselt number because the swirl enhances the turbulent mixing, leading to an increase in the turbulence intensity, which results in the increase of both surface shear and resultant velocity in the swirl channel. Also the swirl flow enhances the heat transfer due to the circulation of the fluid on account to centrifugal convection as the low density hot fluid at the wall be displaced into the cooler stream. The Nusselt number (Nu) distribution with respect to Reynolds number (Re) is shown in Figure 26. The figure shows an increasing in Nusselt number with increasing the Reynolds number. The data presented above were used to develop a correlation for Nusselt number in tube annuli with plug (flat swirl) inlet flow. The following relation was suggested as the best fit:

$$Nu_t = 0.019125 Re^{0.80742} [1.0+0.3167289 \tan(\beta)]$$

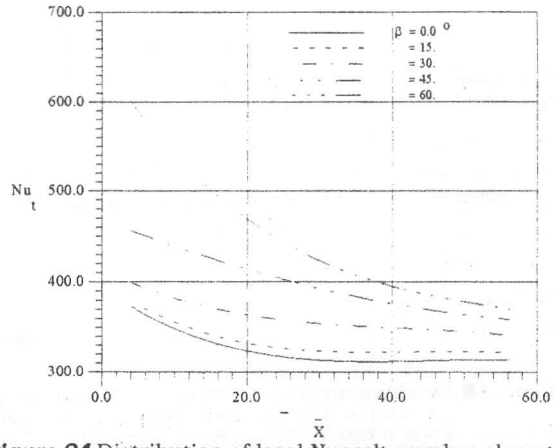

Figure 24 Distribution of local Nusselt number along top wall at different swirl angles. (inlet plug profile, Re=1.66E+05)

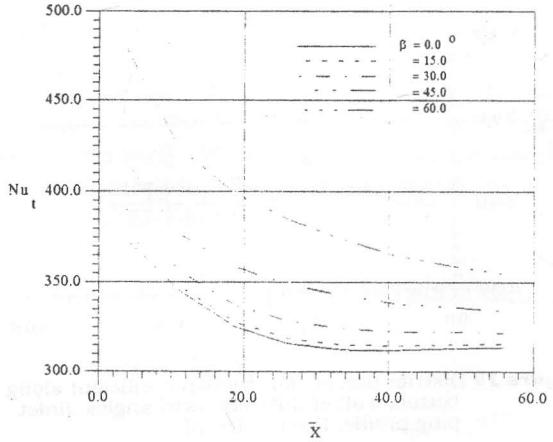

Figure 25 Distribution of local Nusselt number along top wall at different swirl angles. (inlet solid body rotation profile, Re=1.66E+05)

This relation is related to the Nusselt number with swirl angle and is compared with the previous relation of Garimella *et al.* [17], for smooth annuli as shown in Figure 26.The effect of varying the annulus ratio (DR) on the Nusselt number distribution along the top and bottom walls of annular pipe at zero swirl are shown in Figures 27 and 28. The results show that increasing the DR is causes an increase in the Nusselt number. Also, it shows a cross-over at $\overline{X}$ = 41.26.

To validate the present results, a comparison with previous findings [17] has been conducted and presented in Figure 21 for the skin friction coefficient and Figure 26 for Nusselt number distribution. The results show good correspondence between the test results and the literature values.

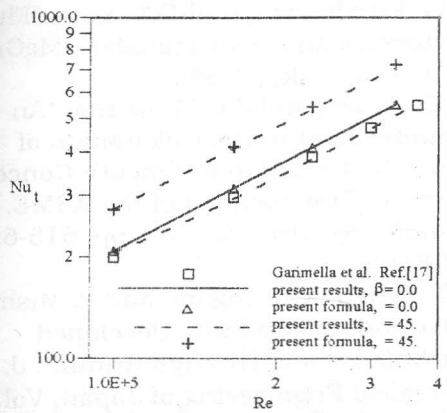

Figure 26 Comparison between predicted Nusselt number and predicted by [17].

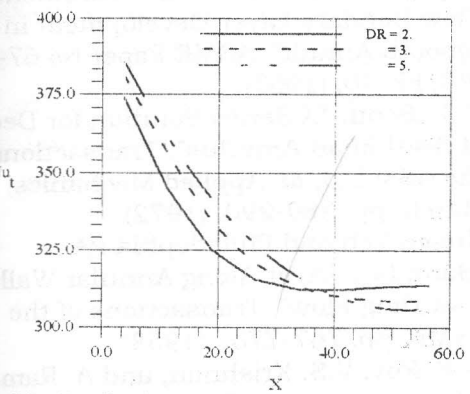

Figure 27 Distribution of Nusselt number along top wall at different diameter ratio. (inlet plug profile, Re=1.66E+05 and β=0.0)

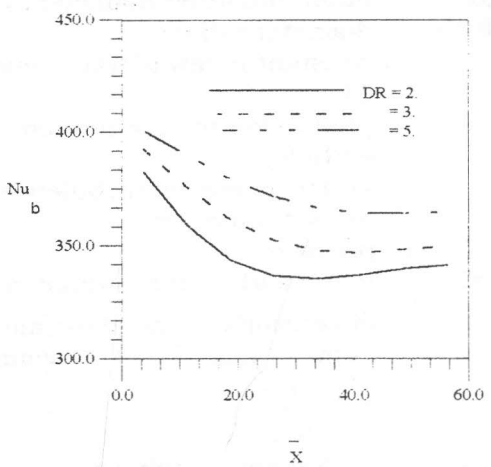

Figure 28 Distribution of local Nusselt number along bottom wall at different diameter ratio. (inlet plug profile, Re=1.66E+05 & β=0.0)

CONCLUSION

The following conclusions can be drawn:

1. The plug flow (flat swirl) inlet profile affects the flow parameters much more than the effect of solid body rotation inlet profile.
2. Friction coefficient along the inner wall is higher than that along the outer wall. The difference in friction coefficients between the outer wall and the inner wall is increased with introducing the swirl. Increasing swirl intensity shows an increase in local skin friction coefficient along the outer wall for the two types of swirl, while on the inner wall the effect is less with plug flow (flat swirl) and no effect with solid body rotation type.
3. The effect of introducing swirl, plug flow (flat swirl) at angle 60 ° on the energy dissipation is more pronounced than solid body rotation flow at the same angle.
4. Introducing a swirl into the axial flow is resulted in increasing of heat transfer coefficient and increased with increasing swirl intensity.
5. The annulus skin friction coefficient and Nusselt number were correlated in terms of swirl angle β and Reynolds number.

NOMENCLATURE

c_f: skin friction coefficient;

c_1, c_2, c_d, c_μ: constants in turbulence model;

D,d: outer and inner diameters;
DR: diameter ratio;
E: constant in law of wall, Equation 11;
G: production term, Equation 8;
h: enthalpy;
k: kinetic energy of turbulence;
Nu: Nusselt number;
p: pressure;
r , x: radial and axial coordinates;
r^* dimensionless radial distance from axis of symmetry, $r^* = \frac{r - r_{in}}{r_{out} - r_{in}}$
Re: Reynolds number;
u, v and w: mean axial, radial and tangential velocity components;
V: velocity vector
$\bar{x}$ dimensionless axial distance, $\bar{x} = \frac{x}{(r_{out} - r_{in})}$:
S_φ : source term of variable φ, Equation 9;
u_{in}: average inlet axial velocity;
u^+: friction velocity Equation 11;
y_p: distance normal to the wall;
y_p^+: dimensionless distance normal to the wall, Equation 11;

Greek Symbols

β: inlet swirl angle;
Γ_φ: exchange coefficient for φ;
ε: dissipation of kinetic energy;
μ: laminar viscosity;
μ_t: turbulence viscosity;
μ_{eff}: effective viscosity;
ν: kinematic viscosity;
ρ: density;
σ_ε , σ_k , σ_h: constants in turbulence model;
τ_t: total shear stress;
τ_w: wall shear stress;
τ_{rx} , $\tau_{r\theta}$: shear stress components;
φ: an arbitrary dependent variable.
χ: constant in law of wall, Eqn.(11);

Subscripts

B: boundary;
b: bottom wall;
eff: effective;
in: inner, inlet;
out: outer;
l: laminar;
p: pole;
t: turbulent, top wall

REFERENCES

1. R.R. Rothfus, C.C. Monrad, and V.E. Senecal, "Velocity Distribution and Fluid Friction in Smooth Concentric Annuli", Ind, Engineering Chem., Vol. 42, pp. 2511-2520 (1950).
2. R.R. Rothfus, W.K. Sartony, R.I. and Kermode, "Flow in Concentric Annuli at high Reynolds number, AICHE Journal, Vol. 12, pp. 1086-1091. (1966)
3. J.G. Kundensen, and D.L. Katz, "Fluid Dynamics and Heat Transfer", McGraw-Hill, New York, (1958).
4. O.C. Jones, and J.C.M. Leung, "An Improvement in the Calculation of Turbulent Friction in Smooth Concentric Annuli", Transactions of the ASME, J. of Fluids Eng. Dec.,Vol.103, pp. 615-623 (1981)
5. R.P. Singh, K.K. Nigam, and P. Mishary, "Developing and Fully Developed Turbulent Flow Through Annuli", J. Chemical Engineering of Japan, Vol.13, No. 5, pp. 349-353 (1980).
6. G.K. Serovy, and Okiishi, "An Experimental Study of the Turbulent Flow Bondary Layer Development in Smooth Annuli", ASME Paper No.67-WA/FE-10, (1967).
7. C.J. Scott, "A Series Solution for Decay of Swirl in an Annulus", Transactions of the ASME, J. of Applied Mechanics, March, pp. 289-290, (1972).
8. Husan Yeh and Philadephia PA., "Boundary Layer Along Annular Walls in a swirling Flow", Transactions of the ASME, pp. 767-776, (1958).
9. R.P. Roy, V.S. Krishnan, and A. Raman, "Measurements in Turbulent Liquid Flow Through a Vertical Concentric Annular Channel", Transactions of the. ASME, J.

Heat Transfer Vol. 108, pp. 216-218, (1986).
10. Jack D. Mattingly and C. Oates Gordon, , "An Experimental Investigation of the Mixing of Coannular Swirling Flows", AIAA, Journal Vol. 24. No. 5, pp. 785-792 (1986).
11. E.E. Khalil D.P. Spalding and J.H. Whitelaw "The Calculation of Local Flow Properties in Two-Dimensional Furnace", Int., Journal Heat Mass Transfer Vol. 18. pp. 775-791, (1975).
12. S.V. Patanker, "Numerical heat transfer and Fluid Flow", Mc Graw-Hill, New York, (1980).
13. A.D. Gosman, E.E. Khalil, and J.H. Whitelaw, "The Calculation of Two-Dimensional Turbulent Recirculating Flows", in Turbulent Shear flows, Edited Durst et al, Springler Verlag, (1979).
14. B.E. Launder, and D.B. Spalding, "The Numerical Compution of Turbulent Flows", Comp. Methods in Appl. Mech. and Engg., Vol. 3, pp. 269-289. (1974)
15. A. Raafat, "Effect of the Pressure Gradient on the Viscous Fluid Flow Pattern" ph.D Thesis, Menoufia University, (1990).
16. B.E. Lounder, and D.B. Spalding, "Mathematical Models of Turbulence", Academic Press, Londn, England, (1972).
17. R.N. Christensen and Garimella, "Heat Transfer and Pressure Drop Characteristics of Spirally Fluated Annuli", Part I Hydrodynamics, Transactions of the ASME, J. of Heat Transfer Vol. 117, pp. 54-60, (1995)

Received June 22.1998
Accepted October 24. 1998

السريان الدوامى الاضطرابى فى القنوات الحلقية

محمد عبد المجيد و مفرح حمادة حامد و فوزى شعبان أبو طالب
قسم هندسة القوى الميكانيكية -جامعة المنوفية

ملخص البحث:

أجريت الدراسة النظرية لخصائص السريان الاضطرابى فى القنوات الحلقية المستقيمة. ولبيان خصائص السريان وانتقال الحرارة فى وجود الدوامات فقد ادخل نوعين من السريان الدوامى عند مدخل القناة إلى السريان المحورى خلالها. وقد تم دراسة تأثير شدة الدوامات ونسبة الأقطار على خصائص السريان وانتقال الحرارة خلال القنوات الحلقية. وقد تم حساب توزيع السرعات والخصائص الاضطرابية للإنسياب ومفاقيد الاحتكاك على الجدران الداخلية والخارجية ورقم النوسلت. والنتائج اظهرت أن الخصائص الاضطرابية للسريان القريب من الجداران الخارجية أعلى منها عند الجدران الداخلية، وأيضا اجهادات القص. كما يكون التحسن فى رقم النولست أعلى مع زيادة شدة الدوامات ومع زيادة نسبة الحلقية(نسبة الأقطار). ومن النتائج تم استنتاج علاقات عددية لكل من معامل الاحتكاك ورقم النولست مع رقم الرينولدز وشدة الدوامات عند المدخل. وقد عقدت مقارنة للنتائج الحالية مع نتائج علاقات مستنتجة لباحثين أخرين سابقين وأظهرت المقارنة درجة مقبولة من التوافق.